Computational Materials Science 115 (2016) 85–91

Contents lists available at ScienceDirect

Computational Materials Science

journal homepage: www.elsevier.com/locate/commatsci

Alloying Mg with Gd and Y: Increasing both plasticity and strength

Lingling Tang [a], Wei Liu [a,*], Zhigang Ding [a], Dalong Zhang [c], Yonghao Zhao [a,*], Enrique J. Lavernia [c], Yuntian Zhu [a,b]

[a] Nano Structural Materials Center, School of Materials Science and Engineering, Nanjing University of Science and Technology, Nanjing 210094, China
[b] Department of Materials Science and Engineering, North Carolina State University, Raleigh, NC 27695, USA
[c] Engineering and Materials Science, University of California, Irvine, CA 92697-1000, USA

ARTICLE INFO

Article history:
Received 7 December 2015
Received in revised form 30 December 2015
Accepted 5 January 2016
Available online 2 February 2016

Keywords:
Magnesium alloys
Plastic deformation
Generalized planar fault energy
Density-functional theory calculations

ABSTRACT

The addition of rare elements to Mg enhances mechanical behavior via solution and precipitation strengthening mechanisms. To provide fundamental insight into the underlying mechanisms, we apply density-functional theory (DFT) calculations to systematically study the generalized planar fault energy (GPFE) for pure Mg and its alloys with Gd, Y, and Gd–Y. Special attention is focused on the $\{0001\}\langle 1\bar{1}00\rangle$ basal and $\{1\bar{1}00\}\langle 11\bar{2}0\rangle$ prismatic slip systems. Our results show that the addition of Gd and Y in Mg significantly reduces the magnitude of GPFE, in particular for the $\{1\bar{1}00\}\langle 11\bar{2}0\rangle$ prismatic slip system. The analysis of the charge density distribution reveals that the predicted reduction in GPFE can be primarily attributed to a decrease of shear resistance between the slip planes. Based on the criterion for the anisotropy of the dislocation mobility and disembrittlement parameter, we demonstrate that alloying Mg with Gd and Y yields lower resistance to slip and hence an improvement in plasticity. Our results also suggest that the strength and plasticity of the Mg–Gd–Y system can be simultaneously enhanced due to charge transfer between Mg and alloying atoms.

1. Introduction

The unique benefits of Magnesium (Mg) alloys, including: low density, ease of machinability, excellent damping capacity and favorable recyclability, render them an ideal material system for applications in the aerospace, aircraft and automotive industries, for example [1]. However, widespread utilization of Mg alloys has been hindered by their poor corrosion/creep resistance and low strength/ductility/plasticity. More recently, published studies suggest that the addition of rare elements to Mg can enhance the mechanical response as a result of solid solution strengthening and precipitation strengthening [2,3]. Studies on Mg–Gd-based alloys show, for example, that strength is influenced, not only by the amount of alloying elements, but also by the processing methodology (*e.g.*, incorporating plastic deformation), and by heat treatment [4–7]. In related work an strengthening effect was reported in an Mg–Gd binary alloy during compression testing and this was attributed to the pining effect of solute atoms on twin boundaries [7]. Moreover, it was reported that Mg–Y alloys have better plasticity than pure Mg because of the activation of additional slip modes [8,9]. In the case of ternary alloys, Mg–Gd–Y systems have been demonstrated to have high tensile yield strength, creep resistance, and corrosion resistance, due to the presence of metastable and stable precipitates that retain their stability at relatively elevated temperatures (up to 250 °C) [10–12]. A typical example of this behavior is provided by the extruded Mg–10Gd–3Y–0.6Zr in weight percentage (in wt.%) alloy [12], which has a ultimate tensile strength (UTS) of 462 MPa and yield strength of 382 MPa. These values are notably greater than those of most AZ series Mg alloys (UTS typically less than 300 MPa). Interestingly, however, and despite the fact that available published studies demonstrate that the strength of Mg can be significantly enhanced by alloying with Gd and Y, strategies to improve the plastic deformation of Mg and its alloys require additional research.

Density-functional theory (DFT) calculations have been widely accepted as a useful tool for understanding the mechanical behavior of metals. By calculating the generalized planar fault energy (GPFE), which indicates the energetic carried upon interrupting the normal stacking sequence of a crystal plane, DFT can predict dislocation core properties at the atomitic level; while at the macroscopic level, it can yield the stress intensity at which dislocations are nucleated at a crack tip [13]. Nowadays, investigation of GPFE in Mg alloys mainly focuses on different binary alloy systems, including Mg with Al, Ca, Cu, Zn, Fe, Mn, Li, Ni, Sn, Y, La, Gd, Nd and Zr [14,15]. In particular, Pei et al. [16] systematically studied GPFE

* Corresponding authors.
E-mail addresses: weiliu@njust.edu.cn (W. Liu), yhzhao@njust.edu.cn (Y. Zhao).

http://dx.doi.org/10.1016/j.commatsci.2016.01.003
0927-0256/

profiles for five systems (*i.e.*, $\{0001\}\langle 11\bar{2}0\rangle$, $\{0001\}\langle 1\bar{1}00\rangle$, $\{10\bar{1}0\}\langle 11\bar{2}0\rangle$, $\{10\bar{1}1\}\langle 11\bar{2}0\rangle$ and $\{11\bar{2}2\}\langle 11\bar{2}3\rangle$) in Mg–Y alloys. Consistent with experimental results, DFT predicted that the addition of Y in Mg enhances the plasticity of Mg, resulting in an alteration in the dislocation core structure and lubrication of the dislocation motion [17,18]. As for Mg–Gd alloys, most theoretical studies have focused on the strengthening effect and stability of precipitated Mg–Gd precipitates, whist neglecting the influence of Gd on GPFE [19]. By using the generalized gradient approximation (GGA) method, Moitra et al. [20] revealed that the addition of Gd to Mg could increase the unstable stacking fault Υ_{usf} value of the $\{0001\}\langle 1\bar{1}00\rangle$ basal plane, but decrease the maximum GPFE value of $\{0001\}\langle 11\bar{2}0\rangle$ basal plane and $\{1\bar{1}00\}\langle 11\bar{2}0\rangle$ prismatic plane. In addition, GPFE investigations in ternary Mg alloy systems have been carried out for Mg–Zn–Y [21], Mg–Al–Zn [22], Mg–Al–Sn [23], and Mg–Zn–Ca [24]. However, GPFE curves of Mg with Gd and Y (Mg–Gd–Y) have not been extensively studied.

In view of the above discussion, in the present work, we study the GPFE curves for four Mg systems: Mg, Mg–6.4Gd, Mg–3.7Y, and Mg–6.2Gd–3.5Y (in wt.%) using DFT calculations, primarily focusing on the $\{0001\}\langle 1\bar{1}00\rangle$ and $\{1\bar{1}00\}\langle 11\bar{2}0\rangle$ slip systems. The $\{0001\}\langle 1\bar{1}00\rangle$ slip system represents the main deformation faults that form in the basal plane because as a result of the slip of partials, 1/3 $\langle 1\bar{1}00\rangle$, while among the prismatic or pyramidal plane slip systems, the $\{1\bar{1}00\}\langle 11\bar{2}0\rangle$ slip system is the easiest to be activated. Both systems are known to play an important role in affecting deformation mechanisms and mechanical properties. Considering that the spacing of (0001) plane is the largest for Mg and that fracture almost always occurs along the basal plane in Mg alloys, the surface energy of (0001) plane was calculated through first-principles rigid tensile tests. Note that the "fixed-grip" method is an universal and accurate approach to determine the surface energy or breaking strength in tensile test for most metal systems [25]. Based on the surface energy and results of GPFE, plasticity was evaluated by the anisotropy of the dislocation mobility and the disembrittlement parameter.

2. Calculation methods

DFT calculations were performed with the Vienna Abinitio Simulation Package (VASP) [26,27]. The Perdue–Burke–Ernzerh (PBE) version [28] was used as the exchange–correlation functional. The projector augmented wave (PAW) method [29] was used to treat interactions between ion cores and valance electrons. The cutoff energy for plane wave basis was set to 350 eV. The total energy accuracy was 5.0×10^{-5} eV atom^{-1}. Brillouin zone sampling was determined using a Gaussian smearing method with the width 0.1 eV and Monkhorst–Pack *k*-point mesh [27] as follows: $3 \times 3 \times 3$ for determining the location of Gd and Y atoms, $9 \times 9 \times 1$ for the GPFE of the $(0001)\langle 1\bar{1}00\rangle$ basal slip system. A *k*-point mesh of $9 \times 7 \times 1$ was used for determining the GPFE curves of the $\{1\bar{1}00\}\langle 11\bar{2}0\rangle$ prismatic slip system and for the first-principles rigid tensile tests. The convergence tests with respect to these parameters showed that the error bar for the total energy is less than 10 meV/atom.

A supercell consisting of 120 atoms was used to locate the Gd and Y atoms in Mg–Gd–Y model. As shown in Fig. 1a, an Mg atom was first substituted by a Gd atom (in red), and then a Y atom (in pink) was used to replace the nearest-neighbor and sub-nearest-neighbor Mg atom of Gd. We considered eleven possible positions for the substitutions, indicated as "Y1" to "Y11" in the figure. In all cases, the atomic positions were optimized with respect to all structural parameters until all Hellman–Feynman forces were less than 0.01 eV/Å. The cohesive energy, E_{coh}, was computed to determine the preferable site for Gd and Y atoms [30]:

$$E_{coh} = (E_{tot} - N_{Mg}E_{Mg} - N_{Gd}E_{Gd} - N_{Y}E_{Y})/(N_{Mg} + N_{Gd} + N_{Y})$$

where E_{tot} is the total energy of the entire system, E_{Mg}, E_{Gd}, and E_{Y} are the single Mg, Gd and Y atoms in an isolated state, respectively. N_{Mg}, N_{Gd}, and N_{Y} denote the number of Mg, Gd and Y atoms in the system, respectively. Our calculations showed that the Y9 site has the lowest cohesive energy and as such, a Y atom located at the Y9 site was used for the Mg–Gd–Y model all through this work. The models for calculating the GPFE of the basal slip system and prismatic slip system are illustrated in Fig. 1b and c, respectively. The supercell contains 12 metal layers with 96 atoms, and a 15 Å vacuum between periodically repeated slabs. Before calculating the GPFE, we compared the Υ_{usf} values to determine the location of Gd and Y atoms. Three positions were calculated: the Gd or Y atom was located in the first, second and third layers below the slip plane. As a result, both in the basal and prismatic slip systems, for Mg–Gd (Y) model, the slip plane was located between the layer containing Gd (Y) atom and the first layer above it (red atoms); in case of Mg–Gd–Y model, the slip plane was located just above the layer containing Y1 (blue atoms).

According to the Rice criterion, the plasticity can be evaluated by combining GPFE results with surface energy [31]. Upon determining GPFE curves, supercell with 96 atoms was performed on first-principles rigid tensile test to calculate the surface energy. There were 12 layers along the $\langle 0001\rangle$ direction, with a vacuum width of 15 Å to avoid image interactions between repeated slabs. The location of Gd and Y was determined in light of the lowest total energy of the considered system. In the Mg–Gd and Mg–Y models, three positions were calculated: the Gd or Y atom was located in the first, second and third layers below the separation plane. In the case of Mg–Gd–Y model, the mentioned three locations above were calculated; moreover, the separation plane that was located between the layers containing Gd and Y was also calculated. Consequently, as shown in Fig. 2a, for Mg–Gd (Y) model, the fracture plane is located between the first layer and the second layer above the layer containing Gd (Y) atom (red atoms); in the case of Mg–Gd–Y model, the location of fracture plane is the second layer above the layer containing Y atom and the third layer above the layer containing Gd atom (blue atoms). The surface energy was obtained by the difference of two total energies in the same system before and after deformation. As seen in Fig. 2b, the tensile deformation was realized through the introduction of 0.8 nm separation distances between two (0001) planes. During calculating, two atomic layers close to the upper and lower free surfaces of the cell were constrained while the calculations the rest atoms were allowed to fully relax.

3. Results and discussion

3.1. GPFE of the basal $\{000\}\langle 1\bar{1}00\rangle$ slip system

Fig. 3 shows the GPFE curves for the basal $\{0001\}\langle 1\bar{1}00\rangle$ slip system of the pure Mg, Mg–Y, Mg–Gd, and Mg–Gd–Y models. The calculated $\Upsilon_{usf}(basal)$ and $\Upsilon_{sf}(basal)$ values of pure Mg model (94 and 34 mJ m^{-2} respectively) are in good agreement with previous studies [32]. For Mg–Y and Mg–Gd models, $\Upsilon_{usf}(basal)$ values are determined to be 72 and 69 mJ m^{-2}, while $\Upsilon_{sf}(basal)$ values are 14 and 12 mJ m^{-2}, respectively. Compared with pure Mg model, the magnitude of $\Upsilon_{usf}(basal)$ for Gd and Y is decreased significantly by 26% and 23%, respectively. As for Mg–Gd–Y model, the $\Upsilon_{usf}(basal)$ and $\Upsilon_{sf}(basal)$ (84 and 21 mJ m^{-2} respectively) are lower than that of pure Mg model and higher than Mg–Y and Mg–Gd models. The $\Upsilon_{usf}(basal)$ value is decreased by 10% and thus presents

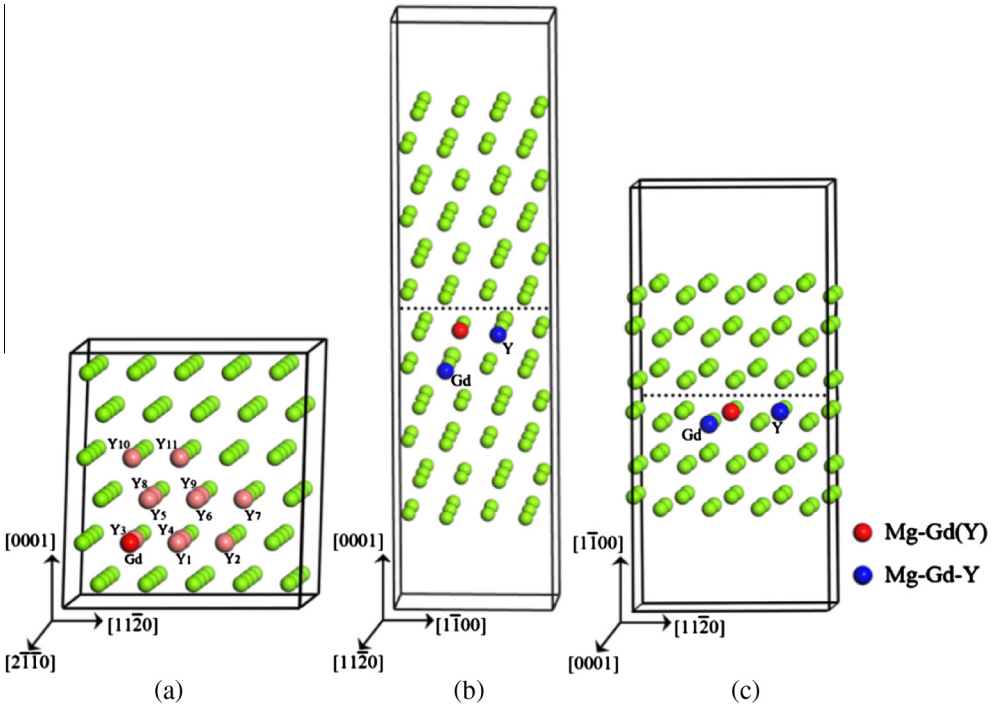

Fig. 1. (a) Mg–Gd–Y model for determining the locations of the Gd and Y atoms; Models used for calculating the generalized planar fault energy for the (b) basal slip system and (c) the prismatic slip system. The dashed line indicates the slip plane.

a *non-linear* characteristic. A similar finding has also been reported in the Mg–Zn–Ca system [24]. In contrast, Zhang et al. [21] reported a linear characteristic of simultaneous addition of Y and Zn, which dramatically decreases the GPFE of the basal $\{0001\}\langle 1\bar{1}00\rangle$ slip system.

In this section we use a typical contour map of charge densities to provide insight into the influence of Gd and Y elements on the GPFE. Notably, the energy profile along a specific pathway is closely related to the charge flows induced by shearing [33]. Three critical states in the GPFE curve were investigated on the $\{0001\}\langle 1\bar{1}00\rangle$ basal slip system: the perfect (denoted as P with stacking sequence ...ABABAB|ABABAB...), the Υ_{usf} (denoted as USF with stacking sequence ...ABABAB|BCBCBC...) and the Υ_{sf} (denoted as SF with stacking sequence ...ABABAB|CACACA...). Fig. 4 shows the charge distribution in the (0002) slip plane in the Mg–Gd and Mg–Y model, which clearly illustrates a relatively high charge density region around Gd and Y. The variation of stacking sequence also significantly affects charge distributions. In the (0002) plane, with the change of the region shape (*i.e.*, from triangular to irregular tetragon and finally to hexagonal), the charge around Gd or Y in states P, USF, and SF exhibits a uniform-distributed trend. In terms of electron density topological theory [34], pure Mg crystal bonds in the pseudo-atom (p-a) type. When adding a Gd or Y atom to the pure Mg, charge transfer occurs from Mg atom to Gd or Y atom, which would partially break the *p-a* type bonding. In addition, alloying systems keep electrical neutrality and the transferred charge is primarily distributed around Gd or Y in the (0002) plane, thus resulting in a reduced interaction between the slip planes. As a result, the associated decrease of slip resistance leads to the decline of GPFE. In addition, the relatively more efficient reduction of GPFE in the Mg–Gd model, relative to that in the Mg–Y model can be attributed to the larger electronegativity of Gd relative to that of Y [35].

Fig. 4c and d ilustrates the charge density distribution in the (0002) planes corresponding to the Mg–Gd–Y models. Clearly, the charge distribution in the (0002) plane containing Gd remains unchanged with a triangular morphology; whereas in the case of the (0 0 0 2) planes where Y is located, the charge region morphology changes from triangular to regular tetragonal and finally to hexagonal. In contrast to the Mg–Gd and Mg–Y models, in state P, the charge distribution of Y reveals a difference: a new charge density region formed between the Mg atoms and the nearby Y atoms. When slip occurs and the system transforms into state USF and SF, the charge distributions in the vicinity of Gd and Y are changed. It should be noted that the Y atom is located in the first layer below the slip plane while the location of Gd is the second layer below the slip plane. Due to the difference in electronegativity, more charge is transferred from Mg to the Gd atom than to the Y atom, which limits the effectiveness of Y to reduce the GPFE.

3.2. GPFE of the prismatic $\{1\bar{1}00\}\langle 11\bar{2}0\rangle$ slip system

The GPFE curves for the $\{1\bar{1}00\}\langle 11\bar{2}0\rangle$ prismatic slip system of four investigated models are shown in Fig. 5. The Υ_{usf} values of prismatic slip, $\Upsilon_{usf}(prism)$, along with $\Upsilon_{usf}(basal)$ and $\Upsilon_{sf}(basal)$ of the pure Mg, Mg–Y, Mg–Gd, and Mg–Gd–Y models, are summarized in Table 1. For pure Mg, the $\Upsilon_{usf}(prism)$ value of 221 mJ m^{-2} is in good agreement with previous DFT studies (218 mJ m^{-2} [36], 225 mJ m^{-2} [37] and 231 mJ m^{-2} [16]). Compared with pure Mg, the $\Upsilon_{usf}(prism)$ values for Mg–Gd and Mg–Y are dramatically reduced by 30% (154 mJ m^{-2}) and 28% (159 mJ m^{-2}), respectively. In the case of Mg–Gd–Y model, the $\Upsilon_{usf}(prism)$ value is 176 mJ m^{-2}, which decreased by 20% compared with that of pure Mg. Therefore, the reduction of GPFE is more effective in the $\{1\bar{1}00\}\langle 11\bar{2}0\rangle$ prismatic slip system than in the $\{0001\}\langle 1\bar{1}00\rangle$ basal slip system. In addition, the reduction trend of GPFE in Mg–Gd, Mg–Y and Mg–Gd–Y models is similar for the basal and prismatic slip systems.

To provide insight into the variation of GPFE in the $\{1\bar{1}00\}\langle 11\bar{2}0\rangle$ prismatic slip system, we now study the charge density in state P and USF in the aforementioned models. Fig. 6a and b shows the charge density distribution in the (1100) plane of Mg–Gd and

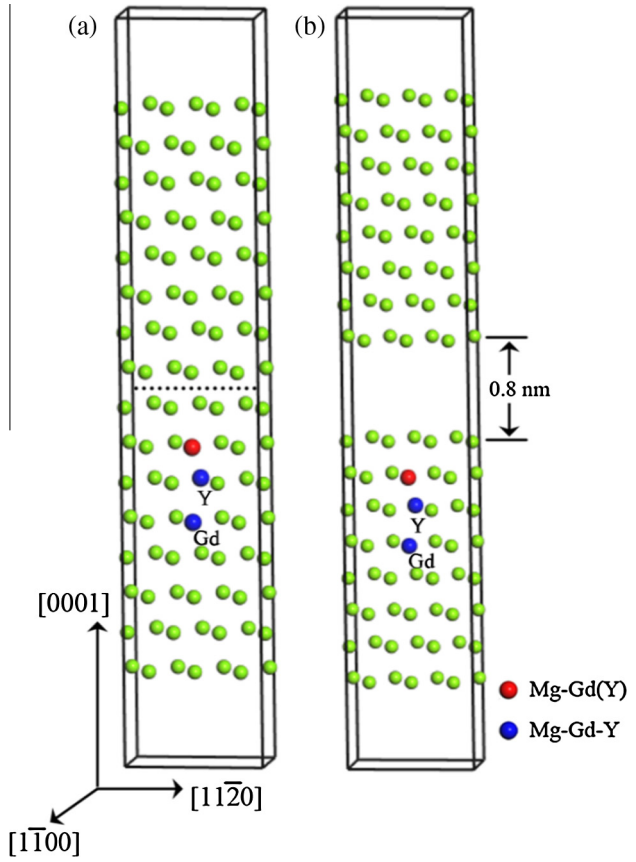

Fig. 2. Models used for calculating the surface energy of the (0001) plane: (a) before tensile deformation and (b) after tensile deformation. In the Mg–Gd and Mg–Y model, locations of Gd and Y atom are indicated by red atoms; in the Mg–Gd–Y model, the locations of Gd and Y atoms are indicated by blue atoms. The dashed line indicates separation plane. (For interpretation of the references to color in this figure legend, the reader is referred to the web version of this article.)

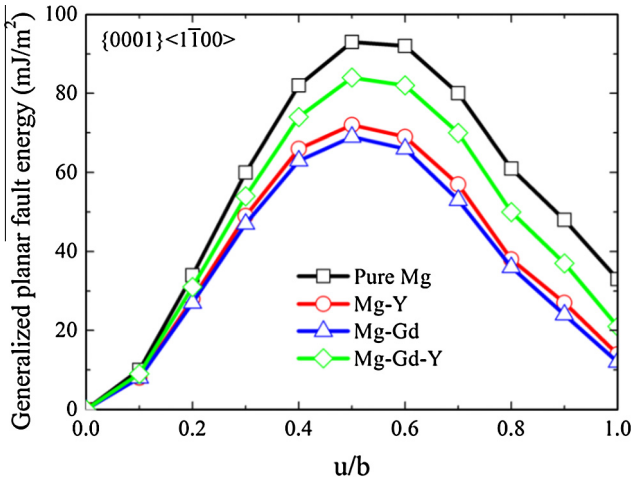

Fig. 3. Generalized planar fault energy curves for the basal {0001}⟨1$\bar{1}$00⟩ slip system of the pure Mg, Mg–Y, Mg–Gd and Mg–Gd–Y models.

Mg–Y models. In state P, the charge distribution of Gd shows a similar tetragonal morphology with Y. When slipping to state USF, narrow bands are formed between the Gd atom and its nearest Mg atoms on both sides. Within the bands, one can see three small high charge density spots along the [0001] direction. Viewed in the [0001] direction, low charge density areas appear between

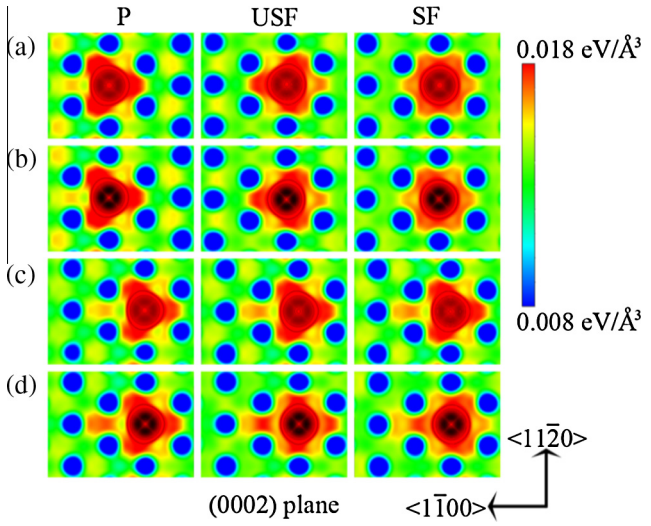

Fig. 4. Maps of charge density from P, USF to SF in the (0002) plane containing (a) Gd atom in the Mg–Gd model; (b) Y atom in the Mg–Y model; (c) Gd atom in the Mg–Gd–Y model and (d) Y atom in the Mg–Gd–Y model. Note that P, USF, and SF refer to the perfect, the unstable stacking fault, and the stable stacking fault state, respectively.

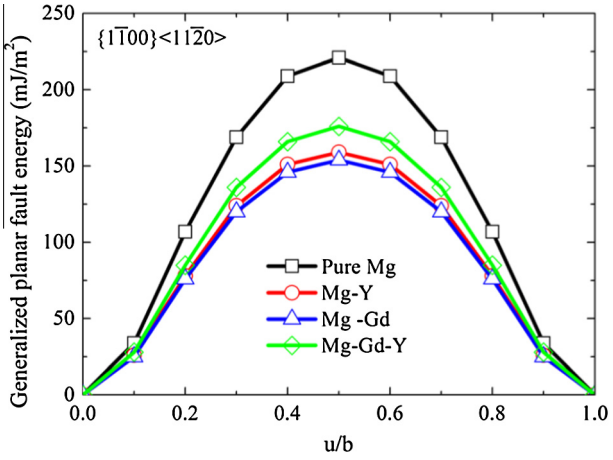

Fig. 5. Generalized planar fault energy curves for the prismatic {1$\bar{1}$00}⟨11$\bar{2}$0⟩ slip system of the pure Mg, Mg–Y, Mg–Gd and Mg–Gd–Y models.

Table 1
Stable stacking fault energies Υ_{sf} and unstable stacking fault energies Υ_{usf} for the basal {0001}⟨1$\bar{1}$00⟩ slip system, $\Upsilon_{sf}(basal)$ and $\Upsilon_{usf}(basal)$, unstable stacking fault energies Υ_{usf} for the prismatic {1$\bar{1}$00}⟨11$\bar{2}$0⟩ slip system, $\Upsilon_{usf}(prism)$, and the ratio of the unstable stacking fault energies, $\Upsilon_{usf}(basal)/\Upsilon_{usf}(prism)$, for the four investigated Mg models (unit: mJ m^{-2}).

	$\Upsilon_{sf}(basal)$	$\Upsilon_{usf}(basal)$	$\Upsilon_{usf}(prism)$	$\Upsilon_{usf}(basal)/\Upsilon_{usf}(prism)$
Pure Mg	34	93	221	0.42
Mg–Y	14	72	159	0.45
Mg–Gd	12	69	154	0.45
Mg–Gd–Y	21	84	176	0.48

the Mg atoms compared with state P, suggesting the charge transfer from the (1100) planes. Fig. 6c and d displays the charge density distributions of Gd and Y in Mg–Gd–Y model, respectively, from which a high charge density region appears at interstitial site and partially connects to the charge area of Gd (Y). Notably, the Gd atom is located at the interstitial site in the lower layer containing Y atom, resulting in an arrangement that provides the impression that Gd and Y are located in the same (1100) plane. In state USF,

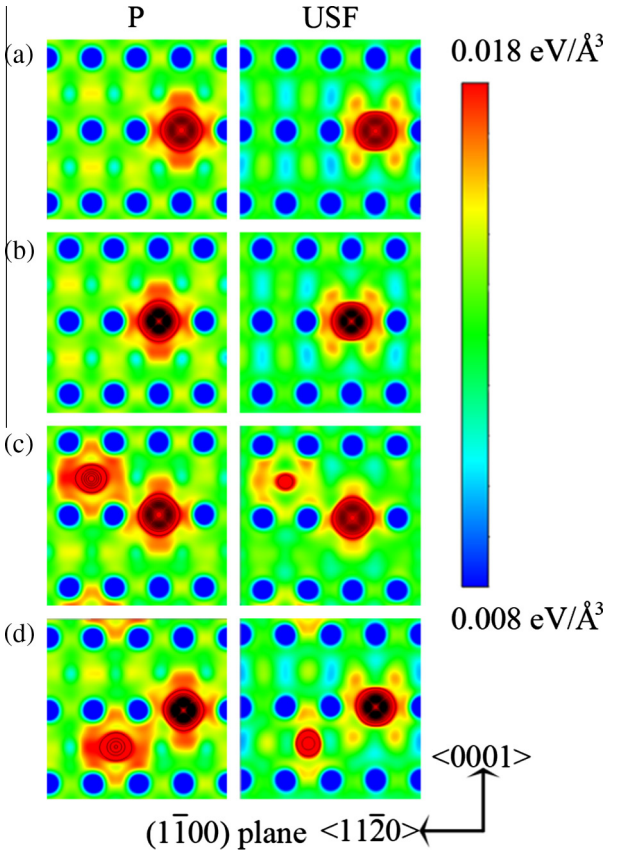

Fig. 6. Maps of charge density from P to USF in the (1100) plane containing (a) Gd atom in the Mg–Gd model; (b) Y atom in the Mg–Y model; (c) Gd atom in the Mg–Gd–Y model and (d) Y atom in the Mg–Gd–Y model.

the charge distribution of Y appears as narrow bands, remaining unchanged relative to that in the Mg–Y model. However, the charge distribution of Gd reveals obvious differences from that in the Mg–Gd model, as the narrow bands change into a faint tetragon. At the same time, the high charge density region formed at interstitial site almost shrinks into a spot for both the Mg–Gd and Mg–Y models.

The stacking sequence of state P in the $\{1\bar{1}00\}\langle 11\bar{2}0\rangle$ prismatic slip system is known to be . . .ABCDAB|CDABCD. . . and in state USF, it stacks in the sequence of . . .ABCDAB|ABCDAB. . . when one half of the $(1\bar{1}00)$ planes slid across the second half to the 1/2 $\langle 11\bar{2}0\rangle$ position [38]. The spacing distance between the (1100) planes is 0.92 Å, which is about one third of the spacing distance between the (0002) planes (2.59 Å). The small spacing distance facilitates the charge transfer along the direction pendicular to the (1100) slip plane. According to the discussion on the $\{0001\}\langle 1\bar{1}00\rangle$ basal slip system, the GPFE should increase in state USF. Considering the change of spacing distance, it is necessary to observe the charge distribution in the (0002) planes. As displayed in Fig. 7a and b, the charge distribution of Gd and Y partially extend to the layer above the slip plane in state P; while in state USF, the charge density of Gd and Y significantly declines and a new high charge density region forms right above the location of the Gd (Y) atom. Although the charge is primarily distributed in the (0001) planes, the interaction between the upper and lower layers of the slip plane actually decreases, leading to the reduction of GPFE in the Mg–Gd and Mg–Y models. In the Mg–Gd–Y system, charge is transferred to the Gd atom and becomes distributed mainly below the location of Gd, resulting in the reduced charge of the Y atom, as shown in Fig. 7c and d. The charge redistribution of Gd and Y atoms can be further confirmed by the high charge density regions

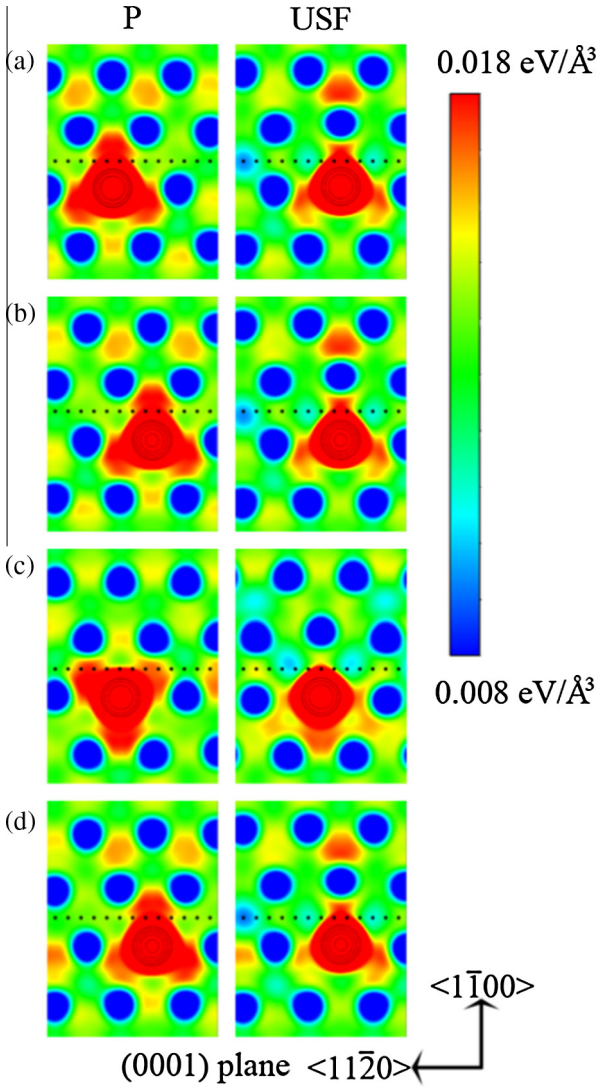

Fig. 7. Maps of charge density from P to USF in the (0001) plane containing (a) Gd atom in the Mg–Gd model; (b) Y atom in the Mg–Y model; (c) Gd atom in the Mg–Gd–Y model and (d) Y atom in the Mg–Gd–Y model. The dashed lines indicate the slip plane.

formed at interstitial site in the (1100) plane (see Fig. 6c and d). The effect of Y atom in reducing the GPFE declines. As a consequence, the GPFE of Mg–Gd–Y system increases. Compared with basal slip system, charge redistribution happens in a larger region in the plane pendicular to the slip plane for the prismatic slip system, which destroys more p-a type bondings. Therefore, an efficient reduction of GPFE can be obtained in the $\{1\bar{1}00\}\langle 11\bar{2}0\rangle$ prismatic slip system. Based on the above discussion, the distance of two slip planes plays a dominant role in determining the charge density distribution.

3.3. Influence of Gd and Y on plastic deformation ability

As discussed in Sections 3.1 and 3.2, a decline of the GPFE values could facilitate dislocation nucleation in both the basal and prismatic planes. Moreover, a significant decrease of GPFE values in the $\{1\bar{1}00\}\langle 11\bar{2}0\rangle$ prismatic slip system can accelerate the activation of nonbasal slip systems, leading to a decrease of plastic anisotropy. Based on the criterion of anisotropy of the dislocation mobility developed by Legrand [39], $\Upsilon_{usf}(basal)/\Upsilon_{usf}(prism)$ could be used to evaluate the anisotropy in Mg. The symmetry of Mg is improved when the ratio is closer to one [40], due to the reduced

Table 2
Surface energies of the four investigated Mg models (unit: mJ m^{-2}).

	Surface energy
Pure Mg	544
Mg–Y	548
Mg–Gd	547
Mg–Gd–Y	558

Table 3
D parameters of the four investigated Mg models. The disembrittlement parameter *D* is the ratio of the surface energy to the unstable stacking fault energy, Υ_{usf}.

	D parameters
Pure Mg	5.85
Mg–Y	7.61
Mg–Gd	7.93
Mg–Gd–Y	6.64

basal plane texture. $\Upsilon_{usf}(basal)/\Upsilon_{usf}(prism)$ in pure Mg, Mg–Y, Mg–Gd, and Mg–Gd–Y models are listed in Table 1. The ratio in the Mg–Gd–Y model is 0.48, which is the closest to one, and it clearly demonstrates the greatest reduction of plastic anisotropy in the Mg–Gd–Y model.

A reduction of GPFE values in these two slip systems could also improve plasticity. Based on Rice's criterion [31], Mehl et al. [41] developed and defined the disembrittlement parameter *D* as the ratio of the surface energy to the Υ_{usf}, which was applied to explain the plasticity problems in faced-centred cubic metals. As reported in Ref. [25], the surface energy can be obtained by the first-principle rigid tensile test and can serve as a measure for the resistance against crack initiation and growth. For the four investigated models, the surface energy values are listed in Table 2. The four values are close and the largest value (*i.e.*, 558 mJ m^{-2}) is obtained in the Mg–Gd–Y model. Hence, on the basis of our calculations, we propose that the Mg–Gd–Y system provides the best resistance to crack initiation and propagation. In other words, a higher external stress is needed to form a fresh surface. Therefore, the surface energy can be also applied to estimate the fracture strength of materials. Among the four models studied herein, the Mg–Gd–Y system is predicted to offer the highest fracture strength. The calculated disembrittlement parameters summarized in Table 3 are 5.85, 7.61, 7.93, and 6.64 for the pure Mg, Mg–Y, Mg–Gd, and Mg–Gd–Y model, respectively. These data show a similar tendency with the decrease of Υ_{usf} values in both the basal and prismatic slip system, indicating that the disembrittlement parameter *D* is strongly dependent on Υ_{usf} rather than on the surface energy. In theory, the Mg–Gd model displays better plasticity than the other three. The value of Mg–Gd–Y model is higher than that of pure Mg and smaller than that of the Mg–Y and Mg–Gd models. In terms of achieving a combination of high strength and plasticity, the Mg–Gd–Y system is the most promising. Therefore, through alloying Gd and Y, an improvement in the plasticity deformation of Mg can be anticipated. In addition, by studying the Mg–Gd, Mg–Y, and Mg–Gd–Y models, our work suggests that the disembrittlement parameter *D* is also suitable to evaluate the ductile *vs.* brittle behavior for the hexagonal close-packed structure of Mg.

4. Conclusions

DFT calculations of the GPFE for the $\{0001\}\langle 1\bar{1}00\rangle$ basal and $\{1\bar{1}00\}\langle 11\bar{2}0\rangle$ prismatic slip systems, and the surface energy of the (0001) plane are performed in pure Mg and its alloys (Mg–Gd, Mg–Y and Mg–Gd–Y). Our calculations demonstrate that the addition of Gd and Y can decrease the GPFE of the two slip systems, in particular for the $\{1\bar{1}00\}\langle 11\bar{2}0\rangle$ prismatic slip system. The analysis of charge density reveals that the reduced GPFE can be attributed to the decreased shear resistance between slip planes and that the spacing between the two slip planes plays a dominant role in determining the charge redistribution. The surface energy results showed that alloying with Gd and Y could improve the ability of inhibiting crack initiation and propagation. Based on the criterion for the anisotropy of the dislocation mobility and the disembrittlement parameter *D*, alloying with Gd and Y could improve the plasticity. Among the four studied models, the Mg–Gd–Y system is predicted to provide the highest strength with good plasticity.

Acknowledgements

W.L., Y.H.Z., and Y.T.Z. are grateful for support from the National Natural Science Foundation of China (Nos. 21403113, 51225102, and 2012CB932203), the Fundamental Research Funds for the Central Universities (No. 30915011330), the Natural Science Foundation for Distinguished Young Scholars of Jiangsu Province (No. BK20150035), the Foundation of Jiangsu Specially-Appointed Professor, and the Pangu Foundation. D.Z. and E.J.L. acknowledge support from NSF-CMMI-1437327.

References

[1] Z. Yang, J.P. Li, J.X. Zhang, G.W. Lorimer, J. Robson, Acta Metall. Sin-Engl. 21 (2008) 313–328.
[2] B. Smola, Stulıková, J. Pelcova, B.L. Mordike, J. Alloy Comp. 378 (2004) 196–201.
[3] I.H. Jung, M. Sanjari, J. Kim, S. Yue, Scr. Mater. 102 (2015) 1–6.
[4] X.Y. Shi, Y. Liu, D.J. Li, B. Chen, X.Q. Zeng, J. Lu, W.J. Ding, Mater. Sci. Eng. A 630 (2015) 146–154.
[5] Y. Jono, M. Yamasaki, Y. Kawamura, Acta Mater. 82 (2015) 198–211.
[6] H. Zhou, G.M. Cheng, X.L. Ma, W.Z. Xu, S.N. Mathaudhu, Q.D. Wang, Y.T. Zhu, Acta Mater. 95 (2015) 20–29.
[7] J.F. Nie, Y.M. Zhu, J.Z. Liu, X.Y. Fang, Science 340 (2013) 957–960.
[8] D.L. Zhang, B.L. Zheng, Y.Z. Zhou, S. Mahajan, E.J. Lavernia, Scr. Mater. 76 (2014) 61–64.
[9] R. Cottam, J. Robson, G. Lorimer, B. Davis, Mater. Sci. Eng. A 485 (2008) 375–382.
[10] S.M. He, X.Q. Zeng, L.M. Peng, X. Gao, J.F. Nie, W.J. Ding, J. Alloy Comp. 421 (2006) 309–313.
[11] N. Stanford, G. Sha, J.H. Xia, S.P. Ringer, M.R. Barnett, Scr. Mater. 65 (2011) 919–921.
[12] D. Lin, L. Wang, F.Q. Meng, J.Z. Cui, Q.C. Le, T. Nonferr, Met. Soc. China 20 (2010) s421–s425.
[13] U.V. Waghmare, E. Kaxiras, M.S. Duesbery, Phys. Status Solidi B 217 (2000) 545–564.
[14] M. Muzyk, Z. Pakiela, K.J. Kurzydlowski, Scr. Mater. 66 (2012) 219–222.
[15] W.Y. Wang, S.L. Shang, Y. Wang, Z.G. Mei, K.A. Darling, L.J. Kecskes, S.N. Mathaudhu, X.D. Hui, Z.K. Liu, Mater. Res. Lett. 2 (2014) 29–36.
[16] Z. Pei, L.F. Zhu, M. Friák, S. Sandlöbes, J.V. Pezold, H.W. Sheng, C.P. Race, S. Zaefferer, B. Svendsen, D. Raabe, New J. Phys. 15 (2013) 043020.
[17] K. Chen, K.P. Boyle, Phys. Status Solidi B 249 (2012) 2089–2095.
[18] Z.R. Liu, D.Y. Li, Comp. Mater. Sci. 103 (2015) 90–96.
[19] L. Gao, J. Zhou, Z.M. Sun, R.S. Chen, E.H. Han, Chin. Sci. Bull. 56 (2011) 1142–1146.
[20] A. Moitra, S.G. Kim, M.F. Horstemeyer, J. Phys. – Condens. Mater. 26 (2014) 445004.
[21] Q. Zhang, L. Fu, T.W. Fan, B.Y. Tang, L.M. Peng, W.J. Ding, Physica B 416 (2013) 39–44.
[22] C. Wang, H.Y. Wang, H.Y. Zhang, X.L. Nan, E.S. Xue, Q.C. Jiang, J. Alloy Comp. 575 (2013) 423–433.
[23] H.Y. Wang, N. Zhang, C. Wang, Q.C. Jiang, Scr. Mater. 65 (2011) 723–726.
[24] M. Yuasa, M. Hayashi, M. Mabuchi, Y. Chino, Acta Mater. 65 (2014) 207–214.
[25] M. Yamaguchi, Metall. Mater. Trans. A 42 (2011) 319–329.
[26] W. Kohn, L.J. Sham, Phys. Rev. 140 (1965) A1133.
[27] H.J. Monkhorst, J.D. Pack, Phys. Rev. B 13 (1976) 5188.
[28] J.P. Perdew, Phys. Rev. B 33 (1986) 8822.
[29] P.E. Blöchl, Phys. Rev. B 50 (1994) 17953.
[30] C.Y. Geng, C.Y. Wang, T. Yu, Acta Mater. 52 (2004) 5427–5433.
[31] J.R. Rice, J. Mech. Phys. Solids 40 (1992) 239–271.
[32] Z.G. Ding, S. Li, W. Liu, Y.H. Zhao, Adv. Mater. Sci. Eng. 2015 (2015) 639519.
[33] Y. Qi, R.K. Mishra, Phys. Rev. B 75 (2007) 224105.

[34] N. Kioussis, M. Herbranson, E. Collins, M.E. Eberhart, Phys. Rev. Lett. 88 (2002) 125501.
[35] W. Gordy, W.J.O. Thomas, J. Chem. Phys. 24 (1956) 439–444.
[36] J.A. Yasi, T. Nogaret, D.R. Trinkle, Y. Qi, J.L. Hector, W. Curtin, Model Simu. Mater. Sci. Eng. 17 (2009) 055012.
[37] I. Shin, E.A. Carter, Model Simul. Mater. Sci. Eng. 20 (2012) 015006.
[38] P. Kwaśniak, P. Śpiewak, H. Garbacz, K.J. Kurzydłowski, Phys. Rev. B 89 (2014) 144105.
[39] C. Briançon, B. Legrand, R.J. Walen, T. Vylov, A. Minkova, A. Inoyatov, Nucl. Instrum. Meth. Phys. Res. 221 (1984) 547–557.
[40] G. Simmons, H. Wang, Single Crystal Elastic Constants and Calculated Aggregate Properties: A Handbook, Massa-Chusetts Institute of Technology, Cambridge, MA, 1971.
[41] Y. Mishin, M.J. Mehl, D.A. Papaconstantopoulos, A.F. Voter, J.D. Kress, Phys. Rev. B 63 (2001) 224106.